A novel signaling pathway in basal breast cancer involving Lyn and the atypical kinase SgK269/PEAK1

David R. Croucher[1,2], Falko Hochgräfe[1,3], Luxi Zhang[1], Ling Liu[1], Ruth J. Lyons[1], Danny Rickwood[1], Carole M. Tactacan[1], Brigid C. Browne[1], Naveid Ali[1], Howard Chan[1], Robert Shearer[1], David Gallego-Ortega[1], Darren N. Saunders[1], Alexander Swarbrick[1] and Roger J. Daly[1].

1. Cancer Research Program, The Kinghorn Cancer Centre, Garvan Institute of Medical Research, 370 Victoria St, Sydney, NSW 2010, Australia.
2. Current Address: Systems Biology Ireland, University College Dublin, Belfield, Dublin 4, Ireland.
3. Current Address: Junior Research Group Pathoproteomics, Competence Center Functional Genomics, University of Greifswald, Germany

Running Title: The role of SgK269 in basal breast cancer

Keywords: Triple negative, Signal transduction, tyrosine kinase, Pseudokinase, Grb2, Stat3

Corresponding Author:

Prof. Roger J. Daly
The Kinghorn Cancer Centre
Garvan Institute of Medical Research
370 Victoria Street, Darlinghurst
Sydney, NSW 2010, Australia
Email: r.daly@garvan.org.au
Tel: +61-2-9355-5825, Fax: +61-2-9355-5870

Word Count: 5000

Figure Number: 7

Conflict of Interest: No authors have a conflict of interest in relation to submission of this manuscript.

Abstract

We recently identified a prominent Src family kinase (SFK) signaling network in basal breast cancer cells that features high expression of the SFK Lyn. In the current study we used quantitative phosphoproteomic profiling to identify novel Lyn substrates, which included the atypical kinase SgK269, also known as PEAK1. Amongst breast cancer cell lines, SgK269 expression was strongly associated with the basal phenotype, while in primary breast cancers, marked SgK269 overexpression was detected in a subset of basal, HER2 and luminal cancers. In MCF-10A mammary epithelial cells, SgK269 promoted transition to a mesenchymal phenotype and increased cell motility and invasion. In addition, growth of MCF-10A acini in three-dimensional culture was greatly enhanced upon SgK269 over-expression, which also induced an abnormal, multilobular acinar morphology and promoted Erk and Stat3 activation. Importantly, a SgK269 mutant where a major Lyn phosphorylation site, Y635, was mutated to phenylalanine was unable to enhance acinar size or cellular invasion. We demonstrate that Y635 represents a Grb2 binding site that promotes both Stat3 and Erk activation in 3D culture. Knockdown of SgK269 in basal breast cancer cells promoted acquisition of epithelial characteristics and decreased anchorage-independent growth. These studies identify a novel signaling pathway in basal breast cancer involving Lyn and SgK269 that presents opportunities for therapeutic intervention.

Introduction

Basal breast cancers usually exhibit a 'triple-negative' receptor phenotype and are therefore resistant to endocrine or trastuzumab therapy (1). The identification of novel therapeutic targets for this clinically aggressive subgroup represents a high priority. We recently utilised phosphoproteomic profiling to identify a signaling network associated with basal breast cancer cells that is governed by Src family kinases (SFKs) (2). The SFK Lyn was a prominent member of this network, which also contained the atypical kinase Sugen Kinase 269 (SgK269) also termed PEAK1 (3).

SgK269, along with SgK223, comprises the New Kinase Family 3 (NKF3) family of protein kinases. Although both proteins exhibit substitutions within the critical DFG triplet of the kinase domain activation loop, leading to their initial classification as pseudokinases (4, 5), the Klemke group has reported that SgK269 possesses weak tyrosine kinase activity (3). In addition, SgK269 is tyrosine-phosphorylated downstream of several tyrosine kinases (6-11). SgK269 localises to the actin cytoskeleton and focal adhesions and associates with p130Cas and Crk, indicating that it may regulate cytoskeletal organization (3). SgK269 expression is induced by active Ras in a Src-dependent manner, and in pre-clinical models of pancreatic cancer, promotes tumour growth, metastasis and resistance to specific therapies (12).

In this study we refine the network downstream of Lyn in basal breast cancer cells, identifying SgK269 as a target of Lyn phosphorylation. We also characterize the functional role of SgK269 in mammary epithelial and basal breast cancer cells, and determine that Lyn regulates a novel scaffolding function of this kinase.

Materials and Methods

Plasmids. A cDNA encoding N-terminal HA-tagged and C-terminal His/Myc-tagged SgK269 was generated by nested PCR from a human SgK269 cDNA in pCMV6, (Origene) and cloned into the SacII and BamHI restriction sites of the pRetroX-IRES-DsRed Express vector (Clontech). The pSIREN-RetroQ-ZsGreen (Clontech) constructs containing shRNA targeting SgK269 and GFP (negative control) were constructed by the ligation of synthesized oligonucleotides into the BamHI and EcoRI sites of pSIREN. The negative control sequence targeting GFP has been previously described (13). The pLKO.1 (Thermo Fisher) constructs containing shRNA targeting SgK269 and a non-targeting control were generated by the ligation of synthesised oligonucleotides into the AgeI and EcoRI sites of pLKO.1. Oligonucleotide sequences can be provided upon request.

Antibodies and Reagents. All antibodies were from Cell Signaling Technology, except: PY20 (Abcam); SgK269 and Tubulin (Santa Cruz Biotechnology); β-Actin (Sigma); Shc, Grb2 and E-cadherin (BD Biosciences); HA (Roche); GAPDH (Ambion). The affinity purified rabbit antibody selective for SgK269 pY635 was generated by Cambridge Research Biochemicals Ltd (Cleveland, UK) by standard procedures.

Tissue culture and generation of stable cell lines. MCF-10A cells stably expressing the murine ecotropic receptor were maintained as previously described (14). All cancer cell lines were obtained from the American Type Culture Collection, except for MDA-MB-231 and T-47D (EG&G Mason Research Institute) and MCF-7 (Michigan Cancer

Foundation). Cell lines were authenticated by short tandem repeat polymorphism, single nucleotide polymorphism, and fingerprint analyses, passaged for less than 6 months, and cultured as previously described (15). The packaging cell line PlatE was used for retrovirus production, and MCF-10A and breast cancer cells were infected with retrovirus as previously described (13). Stable knockdown of SgK269 expression in MDA-MB-231 cells was achieved by lentiviral-mediated transduction of the corresponding pLKO.1 construct, packaged with VSVG pseudotype in HEK-293 cells, followed by puromycin (0.7 μg/ml) selection. Cell proliferation assays were performed using MTS reagent (13). Live cell microscopy, tracking analysis and invasion assays were as previously described (2, 16).

siRNA treatment. Lyn- and Src-selective siRNAs were obtained from Qiagen and Applied Biosystems, respectively. Sequences can be provided upon request. Negative control siRNA was ON-TARGET*plus* non-targeting pool (Dharmacon). siRNA was applied to cells as previously described (13).

SILAC labeling and phosphoproteomic analysis. BT-549 and MDA-MB-231 cells were subject to 'light' (Arg 0, Lys 0) or 'heavy' (Arg 10, Lys 8) SILAC labelling by standard procedures (17). Ten 80% confluent 15 cm dishes were used per transfection condition. In one experiment, the control and Lyn siRNA-transfected cells were labeled with 'light' and 'heavy' isotopes, respectively. A replicate experiment was then undertaken with the labels switched. Phosphopeptide enrichment using P-Tyr-100 and PY20 antibodies and mass spectrometry analysis was undertaken essentially as

previously described (2, 18). Changes in protein abundance between light and heavy labeled cell populations were determined by tryptic in-gel digestion of SDS PAGE separated protein mixtures following standard procedures. Mass spectra were processed with version 1.1.1.14 of the MaxQuant software package using default settings (19). Phosphosite identifications were filtered for greater than 0.75 localization probability. In order to select an appropriate cut-off for selection of Lyn targets, we plotted the frequency distribution of the SILAC phosphosite fold changes and divided the data into three terciles with different percentage cut-offs (20). A fold change of 1.2 fold was selected as this defined the 75-100% tercile.

Cell lysis, immunoprecipitation and pulldowns. Cell lysates for immunoblotting and immunoprecipitation were prepared using lysis and RIPA buffers, respectively (14). Fusion protein pulldowns and peptide competition assays were performed as previously described (21, 22). The latter used a final concentration of 50 μM peptide.

qPCR analysis The AnalytikJena innuPREP RNA Mini Kit was used to extract mRNA. Reverse transcription was performed with the Reverse Transcription System (Promega). qRT-PCR was performed on an Applied Biosystems ABI 7900 qPCR machine (Absolute Quantification setting) using TaqMan Gene Expression Assays (Applied Biosystems). Standard curves were constructed for each TaqMan probe and data were analysed through the 2-ΔΔCt method, corrected for the efficiency of each TaqMan probe and normalised to the GAPDH housekeeping gene. The RT² Profiler™ PCR Array for Human EMT (Qiagen) was used for gene expression profiling.

Three dimensional growth analysis This was performed in Matrigel (BD Biosciences) (14). Photographs of acini were taken using a Leica DFC280 camera with Leica Firecam software (Version 1.9). Acinar diameter was measured using ImageJ Software (Version 1.37).

Fluorescence microscopy This was performed using a Zeiss Axiovert 200M inverted fluorescence microscope. Digital images were processed using Axiovision software (Version 4.7). Cell preparation and staining was performed as previously described (23).

Anchorage independent growth assays These were undertaken essentially as previously described (2). Resulting colonies were fixed and stained using Diff-Quick (Lab Aids), and photographs taken using a Leica DFC280 camera with Leica Firecam software (Version 1.9). Colonies larger than 30 μm were quantified by visual inspection.

Human breast cancer specimens These were provided by the Victorian Cancer Biobank, which is supported by the Victorian Government. The project was approved by St Vincent's Hospital Sydney Human Research Ethics Committee (approval number HREC 08/145). All breast cancer samples were grade 3 carcinoma and classified by immunohistochemistry as luminal (ER+PR+HER2-), HER2-positive (ER-, PR-, HER2+) and basal (ER-, PR-, HER2-).

Results

Identification of Lyn-regulated tyrosine phosphorylation events in basal breast cancer cells

Previously we determined that basal breast cancer cells are characterized by a prominent SFK signaling network that features high expression of the SFK Lyn (2). To characterise the role of Lyn we undertook quantitative phosphoproteomic profiling of BT549 and MDA-MB-231 cells following siRNA-mediated Lyn knockdown (Figure 1A-C). This identified seven Lyn targets that were common to both cell lines (Figure 1C) (Supplementary Figure 1). Three were present in our previously identified phosphorylation signature (Supplementary Figure 2) (2), specifically Talin-1 (TLN1), α/β-Enolase (ENOA/B) and SgK269, while Annexin A2 (ANXA2) did not appear in the signature but is a known interaction partner and phosphorylation target of Lyn (24). A decrease in phosphorylation of the network component BCAR3 was only detected in MDA-MB-231 cells. Other proteins identified as Lyn substrates in MDA-MB-231 and/or BT549 cells were not present in the previously identified signature, indicating that they do not exhibit differential phosphorylation between luminal and basal breast cancer cells.

In parallel, we used SILAC to profile protein expression changes following Lyn knockdown. For many putative Lyn substrates, including ANXA2, ENOA/B, and TLN1, this revealed that Lyn knockdown results in reduced relative tyrosine phosphorylation of specific sites, rather than decreased protein expression (Supplementary Figure 1). Since SgK269 could not be detected by MS analysis of total protein lysates, we generated a phosphospecific antibody against one of the Lyn-regulated phosphosites identified, Y635 (Supplementary Figure 3A). Western blotting of SgK269 immunoprecipitates using this

antibody confirmed that relative Y635 phosphorylation is markedly reduced following Lyn knockdown (Figure 1D). Of note, this decrease was not apparent if the immunoprecipitates were blotted with an anti-phosphotyrosine antibody, indicating that Y635 and the other Lyn-regulated phosphosite Y616 make a relatively small contribution to overall tyrosine phosphorylation of SgK269 (Supplementary Figure 3B). Overall, these data indicate that Lyn phosphorylates only a small fraction of the previously identified network (Supplementary Figure 2). This finding was substantiated by blotting of cell lysates with anti-phosphotyrosine and phosphospecific antibodies, which did not reveal major changes in overall tyrosine phosphorylation or in site-specific phosphorylation of the known SFK substrates FAK and BCAR1/Cas following Lyn knockdown (Supplementary Figure 4).

To further interrogate Lyn function in basal breast cancer we chose to focus on SgK269, given its recently reported association with several human malignancies (3, 12).

SgK269 expression in breast cancer cell lines and primary breast cancers

Western blotting across breast cancer cell lines revealed that expression of SgK269 is characteristic of the basal phenotype, as observed for Lyn (Figure 2A) (2). However, this pattern of expression is not reflected in the relative mRNA levels (Figure 2B), indicating that elevated SgK269 expression in basal breast cancer cell lines must be mediated via a post-transcriptional or post-translational mechanism. Since the commercial SgK269 antibody is not suitable for immunohistochemistry, we characterized the expression pattern of SgK269 in different subtypes of primary breast cancer by Western blot analysis (Figure 2C). SgK269 was detected in most of the luminal, HER2

and basal breast cancers analysed, and for each cancer subtype, a subset of the specimens (20-40 %) exhibited marked SgK269 overexpression compared to the remainder. Consequently, while SgK269 overexpression does occur in primary basal breast cancers, dysregulation is not restricted to this breast cancer subtype.

SgK269 promotes epithelial to mesenchymal transition in mammary epithelial cells

To characterize the functional role of SgK269, we stably expressed SgK269 in MCF-10A immortalised breast epithelial cells at a level approximately two-fold higher than that in MDA-MB-231 basal breast cancer cells (Figure 3A). This resulted in cells converting to an elongated, mesenchymal morphology (Figure 3B), and was associated with a decreased expression of E-cadherin and an increase in N-cadherin (Figure 3A), indicative of epithelial-to-mesenchymal transition (EMT) (25). To characterize this phenotypic change further, we undertook a comprehensive expression analysis of genes associated with EMT. Of the 63 genes on the array that are normally upregulated during EMT, 12 showed a significant change, and the majority of these (9 out of 12) increased in expression. Amongst the latter class was ZEB2, a known transcriptional repressor of E-Cadherin (26). Of the 21 genes normally downregulated, 8 showed a significant change, and the majority (6 out of 8) exhibited reduced expression (Figure 3C). SgK269-overexpressing cells also exhibited a significant increase in random cell motility (Figure 3D), and fluorescence microscopy revealed that SgK269 localised to cortical actin as well as actin stress fibres and puncta (Figure 3E and Supplementary Figure 5).

SgK269 promotes growth of MCF-10A acini in three-dimensional culture

SgK269 over-expression did not alter the proliferation of MCF-10A cells in monolayer culture (Figure 4A). However, in Matrigel, SgK269 over-expressing cells generated acini approximately twice the diameter of vector controls (Figure 4B) that exhibited a distinct, multi-lobular morphology (Figure 4C) and lacked hollowed lumens (Figure 4D). In addition, late-stage cultures exhibited prominent Ki67 staining (Figure 4D), demonstrating that SgK269 signaling overcomes the proliferative suppression that normally occurs following acinar development (27).

Phosphorylation of SgK269 Y635 controls acinar growth and cell invasion

To determine the role of Lyn-mediated SgK269 phosphorylation, we mutated individual Lyn-regulated phosphosites (Y616 and Y635) to phenylalanine, and expressed the corresponding mutants in MCF-10A cells (Figure 5A). Anti-phosphotyrosine blotting revealed that neither mutation significantly affected overall SgK269 tyrosine phosphorylation, highlighting the presence of other tyrosine phosphorylation sites (Figure 5A). Expression of these mutants resulted in a similar elongated cellular morphology to that observed upon over-expression of wildtype (WT) SgK269 (Figure 5B). Upon 3D culture, mutation of Y616 was still without effect, but SgK269 Y635F was unable to promote acinar growth to the same degree as WT SgK269 (Figure 5C and 5D). SgK269 Y635F-expressing acini still displayed an aberrant, multi-lobular morphology (Figure 5C and 5D), indicating that acinar growth and morphology are regulated by Y635-dependent and –independent pathways, respectively. In transwell assays, overexpression of SgK269 led to increased cell invasion, but this effect was lost with the Y635F mutant (Figure 5E).

Phosphorylation-dependent interactions of SgK269

To determine possible interaction partners for the Lyn phosphosites within SgK269 we utilised NetPhorest (28). Based upon linear amino acid recognition motifs the most likely binding partner for Y635 was the SH2 domain of Grb2 (Posterior probability of 0.51). Immunoprecipitation of WT SgK269 confirmed that it associates with both Shc and Grb2 *in vivo* (Figure 6A), as well as Crk, which has previously been identified as a SgK269 interactor (3). While the interaction between SgK269 and Shc was not altered for the Y635F mutant, the interaction with Grb2 was decreased by ~50 % (Figure 6B). Given that Y616 and Y1188 both reside within consensus binding motifs for the Shc PTB domain, it is likely that residual Grb2 binding by the Y635F mutant occurs indirectly via Shc. Consistent with our data identifying the SFK Lyn as a mediator of Y635 phosphorylation (Figure 1), treatment of basal breast cancer cells with the SFK inhibitor PP2, or Lyn knockdown, led to decreased Y635 phosphorylation and Grb2 association with SgK269 (Figure 6C, 6D). Interestingly, Src knockdown did not affect Y635 phosphorylation, indicating a predominant role for Lyn in regulating phosphorylation of this site, but the greatest degree of Src knockdown slightly reduced SgK269/Grb2 association (Supplementary Figure 6), which may reflect Src-mediated phosphorylation of other sites on SgK269.

In pulldown assays, a GST-Grb2 SH2 fusion protein bound to WT SgK269, but not SgK269 Y635F (Figure 6E). In addition, binding of SgK269 to this fusion protein was competed by a phosphopeptide corresponding to the Y635 phosphorylation site, but not a non-phosphorylated control peptide (Figure 6E). Overall, these data are consistent

with a model where Lyn-mediated phosphorylation of Y635 leads to recruitment of Grb2 via the Grb2 SH2 domain.

Signaling pathway activation downstream of SgK269

For cells grown in monolayer culture, Erk or Akt activation was not altered upon SgK269 overexpression (Figure 7A). However, phosphorylation of Stat3 at Y705 increased ~3 fold, an effect absent upon expression of SgK269 Y635F. We also performed Western blotting on acinar lysates from Matrigel cultures. Under these conditions, SgK269, but not SgK269 Y635F, enhanced phosphorylation of both Erk and Stat3 (Figure 7A).

To determine the contribution of Erk activation downstream of SgK269 to abnormal growth of MCF-10A acini, cells expressing WT SgK269 were grown in Matrigel in the presence of a MEK inhibitor (PD184352). Low concentrations of MEK inhibitor that were able to negate the increased Erk activation induced upon SgK269 overexpression reduced the size of SgK269 over-expressing acini back to that of vector control acini (Figure 7B). However, SgK269-overexpressing acini grown in the presence of the MEK inhibitor still exhibited a multilobular phenotype, indicating that MEK/Erk activation downstream of SgK269 Y635 impacts on acinar growth rather than morphogenesis. Since MCF-10A cells were unable to grow in Matrigel in the presence of low concentrations of the Stat3 inhibitor Stattic (data not shown), we could not determine the functional role of SgK269-mediated Stat3 activation.

SgK269 promotes EMT and anchorage-independent growth in basal breast cancer cells

To extend the insights gained from an overexpression model, we manipulated SgK269 expression and signaling in basal breast cancer cell lines. Stable SgK269 knockdown in MDA-MB-231 cells led to acquisition of a more epithelial morphology, increased expression of E-Cadherin, and reduced levels of both N-Cadherin and Slug, consistent with mesenchymal to epithelial transition. While Erk activation was unchanged, Stat3 activation was markedly reduced (Figure 7C). The knockdown cells also exhibited decreased viability at low serum concentrations (Supplementary Figure 7A). When WT SgK269 was overexpressed in MDA-MB-231 cells, which exhibit relatively high endogenous levels of this protein, a trend for enhanced anchorage-independent growth relative to controls was observed. However, expression of SgK269 Y635F significantly reduced colony formation, indicating a dominant-negative effect of the mutant (Supplementary Figure 7B-C). SgK269 knockdown in BT-549 cells resulted in decreased Stat3 activation, while there was no change in Erk activity (Figure 7D). However, SgK269 knockdown in MDA-MB-468 cells did not alter Stat3 activity, but Erk activity was decreased (Figure 7D). These findings confirm that endogenous SgK269 can modulate Stat3 and Erk signaling, but indicate that the effect on either pathway can be context-dependent. Importantly, the knockdown of SgK269 in BT-549 cells reduced their ability to grow under anchorage-independent conditions (Figure 7D).

Discussion

Recently, we determined that basal breast cancer cells are characterized by a prominent SFK signaling network that features high expression of the SFK Lyn. In this manuscript, we demonstrate that Lyn positively regulates the phosphorylation of a small subset of proteins within this network that includes the atypical kinase SgK269. In addition, we identify novel Lyn-regulated signaling roles for SgK269.

Lyn has been extensively characterized in the haematopoietic system (29, 30), although it also has an emerging role in solid malignancies (2, 31, 32). This study represents the first detailed phosphoproteomic analysis of Lyn substrates in the latter context. Within the haematopoietic compartment Lyn can have both positive and negative regulatory roles in signal propagation, and known Lyn substrates include inhibitory receptors (PIR-B and SIRP-α) and phosphatases (SHP-1 and SHIP-1), the DOK-1 and Gab2 docking proteins, and the adaptor CrkL (29, 30). CrkL represents the only overlap between proteins identified by our screen and these haematopoietic substrates, presumably reflecting the contrasting expression profile of particular Lyn targets in haematopoietic versus epithelial cells as well as that of receptors/scaffolds that regulate access of Lyn to particular substrates. However, a consistent feature of Lyn substrates in both cell types is that they often represent transmembrane proteins or components of plasma membrane-localized signaling complexes. Many of our identified targets are not documented as known substrates of Lyn or other SFKs. These include Ribosomal Subunit 10, ADAM9, TGFR1 and OSMR.

The Klemke group reported a weak *in vitro* tyrosine kinase activity for SgK269 (3), and in recently published work, demonstrated a pro-proliferative role for this activity

(12). However, our study is the first to demonstrate that Lyn-mediated phosphorylation of Y635 imparts a potent scaffolding function to this protein. Phosphorylation of Y635 was required for SgK269 to promote activation of Erk and Stat3 in 3D culture, cell invasion, and acinar growth, and careful titration of a selective MEK inhibitor confirmed the contribution of the MEK-Erk pathway to the latter biological response. Stimulation of Erk activation by SgK269 is consistent with Y635-mediated recruitment of Grb2 leading to Sos-mediated Ras activation, which could occur at cellular sites where SgK269 is in close proximity to the plasma membrane, for example at the cell cortex or focal adhesions (3). However, how Y635 phosphorylation leads to Stat3 activation is unclear at present. Since we have been unable to co-immunoprecipitate SgK269 with Stat3 (Croucher and Daly, unpublished data), SgK269 does not appear to act as a scaffold for Stat3 and the corresponding kinase, but it remains possible that phosphorylated Y635 activates such a kinase either directly, or via Grb2. A candidate intermediary is Syk, since phosphorylated Y635 is predicted to bind the Syk SH2 domains (28, 33). An alternative model involves Y635-dependent sequestration of Grb2 by SgK269 leading to enhanced recruitment and phosphorylation of Stat3 by the EGFR, which could occur because Grb2 and Stat3 compete for the same binding sites on this receptor (34).

Aside from promotion of acinar growth, the other major effect induced by SgK269 in MCF-10As was acquisition of an elongated and highly motile phenotype, and perturbed acinar morphogenesis. Interestingly, these effects do not appear to be driven by effects of SgK269 on Erk or Stat3 signaling, since Erk activation was not affected by SgK269 in monolayer culture, inhibition of MEK/Erk signaling attenuated growth, but not aberrant morphogenesis, of SgK269-overexpressing acini, and SgK269 Y635F, which

does not promote Stat3 or Erk activation, still altered cell morphology in monolayer and 3D culture. In addition, SgK269-induced morphological effects were independent of Y616 phosphorylation. The most likely explanation for these effects is that SgK269 perturbs cytoskeletal organization, either by directly phosphorylating regulators of the actin cytoskeleton, and/or its scaffolding function. Consistent with this hypothesis, SgK269 associates with Crk and BCAR1/p130Cas (3), known regulators of Rac and Rap GTPases and hence cell spreading and migration (35). Furthermore, in addition to Y616 and Y635, SgK269 contains further known and predicted sites of tyrosine phosphorylation, including Y387, Y641 and Y1188 (2, 3) that could recruit SH2 or PTB domain-containing effectors. Either the direct (kinase-dependent) or indirect (scaffolding) signaling mechanism would be facilitated by localization of SgK269 to the actin cytoskeleton. Overall, our data highlight the capacity of SgK269 to generate several different signal outputs and thereby modulate both cell proliferation and migration.

Importantly, our functional characterization of SgK269 in basal breast cancer cells supports the pathophysiological relevance of data from the MCF-10A model. This demonstrated that SgK269 is required for maintenance of a mesenchymal phenotype in MDA-MB-231 cells, and promotes Stat3 or Erk activation, depending on the cell line. In addition, SgK269 enhanced anchorage-independent growth, a key characteristic of the transformed phenotype, and this activity was dependent on Y635 phosphorylation. Finally, our finding that the invasive potential of SgK269-overexpressing MCF-10A cells, which express high levels of Lyn (our unpublished data), is dependent on Y635 phosphorylation is consistent with our previous observation that Lyn knockdown markedly reduces invasion of basal breast cancer cells (2).

Our characterization of the network roles of Lyn and SgK269 highlights potential strategies for improved treatment of basal breast cancers, as well as other breast cancer subtypes where SgK269 is overexpressed. SgK269 kinase activity may represent a target for therapeutic intervention with small molecule kinase inhibitors, and if SgK269 activates Stat3 via an indirect mechanism, then Stat3 kinases that act downstream of SgK269 may also represent therapeutic targets. Finally, given its signaling role downstream of multiple tyrosine kinases (6-11), and recent data demonstrating that SgK269 modulates cellular sensitivity to Trastuzumab (12), it will be interesting to determine whether SgK269 represents a biomarker of therapeutic responsiveness that could be used for improved patient stratification for targeted therapy.

Acknowledgements and Grant Support: This work was supported by research grants from the National Health and Medical Research Council of Australia, Cancer Council New South Wales (NSW) and Science Foundation Ireland (Grant No. 06/CE/B1129). DRC and DS were supported by Fellowships from Cancer Institute (CI) NSW. FH is supported by The Ministry of Education and Research, Bundesministerium für Bildung und Forschung (03Z1CN21). CMT is the recipient of a Research Scholarship from CINSW, and LZ an Australian Postgraduate Award. DGO is supported by a National Breast Cancer Foundation (NBCF) and Cure Cancer Australia Foundation Postdoctoral Fellowship. AS is supported by an Early Career Fellowship from the NBCF.

References

1. Rakha EA, Reis-Filho JS, Ellis IO. Basal-like breast cancer: a critical review. J Clin Oncol 2008; 26: 2568-81.
2. Hochgrafe F, Zhang L, O'Toole SA, et al. Tyrosine phosphorylation profiling reveals the signaling network characteristics of Basal breast cancer cells. Cancer Res 2010; 70: 9391-401.
3. Wang Y, Kelber JA, Tran Cao HS, et al. Pseudopodium-enriched atypical kinase 1 regulates the cytoskeleton and cancer progression [corrected]. Proc Natl Acad Sci U S A 2010; 107: 10920-5.
4. Manning G, Whyte DB, Martinez R, Hunter T, Sudarsanam S. The protein kinase complement of the human genome. Science (New York, NY 2002; 298: 1912-34.
5. Boudeau J, Miranda-Saavedra D, Barton GJ, Alessi DR. Emerging roles of pseudokinases. Trends Cell Biol 2006; 16: 443-52.
6. Leroy C, Fialin C, Sirvent A, et al. Quantitative phosphoproteomics reveals a cluster of tyrosine kinases that mediates SRC invasive activity in advanced colon carcinoma cells. Cancer research 2009; 69: 2279-86.
7. Luo W, Slebos RJ, Hill S, et al. Global impact of oncogenic Src on a phosphotyrosine proteome. Journal of proteome research 2008; 7: 3447-60.
8. Bonnette PC, Robinson BS, Silva JC, et al. Phosphoproteomic characterization of PYK2 signaling pathways involved in osteogenesis. J Proteomics 2010; 73: 1306-20.
9. Boersema PJ, Foong LY, Ding VM, et al. In-depth qualitative and quantitative profiling of tyrosine phosphorylation using a combination of phosphopeptide immunoaffinity purification and stable isotope dimethyl labeling. Mol Cell Proteomics 2010; 9: 84-99.
10. Zhang G, Fenyo D, Neubert TA. Screening for EphB signaling effectors using SILAC with a linear ion trap-orbitrap mass spectrometer. Journal of proteome research 2008; 7: 4715-26.
11. Guo A, Villen J, Kornhauser J, et al. Signaling networks assembled by oncogenic EGFR and c-Met. Proceedings of the National Academy of Sciences of the United States of America 2008; 105: 692-7.
12. Kelber JA, Reno T, Kaushal S, et al. KRas induces a Src/PEAK1/ErbB2 kinase amplification loop that drives metastatic growth and therapy resistance in pancreatic cancer. Cancer Res 2012; 72: 2554-64.
13. Croucher DR, Rickwood D, Tactacan CM, Musgrove EA, Daly RJ. Cortactin modulates RhoA activation and expression of Cip/Kip cyclin-dependent kinase inhibitors to promote cell cycle progression in 11q13-amplified head and neck squamous cell carcinoma cells. Mol Cell Biol 2010; 30: 5057-70.
14. Brummer T, Schramek D, Hayes VM, et al. Increased proliferation and altered growth factor dependence of human mammary epithelial cells overexpressing the Gab2 docking protein. J Biol Chem 2006; 281: 626-37.
15. deFazio A, Chiew YE, Sini RL, Janes PW, Sutherland RL. Expression of c-erbB receptors, heregulin and oestrogen receptor in human breast cell lines. Int J Cancer 2000; 87: 487-98.

16. Herrera Abreu MT, Hughes WE, Mele K, et al. Gab2 regulates cytoskeletal organization and migration of mammary epithelial cells by modulating RhoA activation. Mol Biol Cell 2011; 22: 105-16.
17. Ong SE, Blagoev B, Kratchmarova I, et al. Stable isotope labeling by amino acids in cell culture, SILAC, as a simple and accurate approach to expression proteomics. Mol Cell Proteomics 2002; 1: 376-86.
18. Rush J, Moritz A, Lee KA, et al. Immunoaffinity profiling of tyrosine phosphorylation in cancer cells. Nat Biotechnol 2005; 23: 94-101.
19. Cox J, Mann M. MaxQuant enables high peptide identification rates, individualized p.p.b.-range mass accuracies and proteome-wide protein quantification. Nat Biotechnol 2008; 26: 1367-72.
20. Pan C, Kumar C, Bohl S, Klingmueller U, Mann M. Comparative proteomic phenotyping of cell lines and primary cells to assess preservation of cell type-specific functions. Mol Cell Proteomics 2009; 8: 443-50.
21. Lowenstein EJ, Daly RJ, Batzer AG, et al. The SH2 and SH3 domain-containing protein GRB2 links receptor tyrosine kinases to ras signaling. Cell 1992; 70: 431-42.
22. Janes PW, Lackmann M, Church WB, Sanderson GM, Sutherland RL, Daly RJ. Structural determinants of the interaction between the erbB2 receptor and the Src homology 2 domain of Grb7. J Biol Chem 1997; 272: 8490-7.
23. Croucher DR, Saunders DN, Stillfried GE, Ranson M. A structural basis for differential cell signalling by PAI-1 and PAI-2 in breast cancer cells. Biochem J 2007; 408: 203-10.
24. Matsuda D, Nakayama Y, Horimoto S, et al. Involvement of Golgi-associated Lyn tyrosine kinase in the translocation of annexin II to the endoplasmic reticulum under oxidative stress. Exp Cell Res 2006; 312: 1205-17.
25. Gravdal K, Halvorsen OJ, Haukaas SA, Akslen LA. A switch from E-cadherin to N-cadherin expression indicates epithelial to mesenchymal transition and is of strong and independent importance for the progress of prostate cancer. Clin Cancer Res 2007; 13: 7003-11.
26. Peinado H, Olmeda D, Cano A. Snail, Zeb and bHLH factors in tumour progression: an alliance against the epithelial phenotype? Nat Rev Cancer 2007; 7: 415-28.
27. Debnath J, Muthuswamy SK, Brugge JS. Morphogenesis and oncogenesis of MCF-10A mammary epithelial acini grown in three-dimensional basement membrane cultures. Methods 2003; 30: 256-68.
28. Miller ML, Jensen LJ, Diella F, et al. Linear motif atlas for phosphorylation-dependent signaling. Sci Signal 2008; 1: ra2.
29. Hibbs ML, Harder KW. The duplicitous nature of the Lyn tyrosine kinase in growth factor signaling. Growth Factors 2006; 24: 137-49.
30. Scapini P, Pereira S, Zhang H, Lowell CA. Multiple roles of Lyn kinase in myeloid cell signaling and function. Immunol Rev 2009; 228: 23-40.
31. Choi YL, Bocanegra M, Kwon MJ, et al. LYN is a mediator of epithelial-mesenchymal transition and a target of dasatinib in breast cancer. Cancer Res 2010; 70: 2296-306.

32. Park SI, Zhang J, Phillips KA, et al. Targeting SRC family kinases inhibits growth and lymph node metastases of prostate cancer in an orthotopic nude mouse model. Cancer Res 2008; 68: 3323-33.
33. Uckun FM, Qazi S, Ma H, Tuel-Ahlgren L, Ozer Z. STAT3 is a substrate of SYK tyrosine kinase in B-lineage leukemia/lymphoma cells exposed to oxidative stress. Proceedings of the National Academy of Sciences of the United States of America; 107: 2902-7.
34. Zhang T, Ma J, Cao X. Grb2 regulates Stat3 activation negatively in epidermal growth factor signalling. Biochem J 2003; 376: 457-64.
35. Defilippi P, Di Stefano P, Cabodi S. p130Cas: a versatile scaffold in signaling networks. Trends Cell Biol 2006; 16: 257-63.

Figure Legends

Figure 1: Phosphoproteomic analysis of basal breast cancer cell lines following Lyn knockdown. (A) Phosphoproteomic profiling workflow. (B) Validation of Lyn knockdown by Western blotting. (C) Venn diagram displaying proteins identified as Lyn substrates in BT-549 and MDA-MB-231 cells. (D) Biochemical confirmation of Lyn-dependent phosphorylation of SgK269 on Y635. SgK269 immunoprecipitates were Western blotted using a pY635 phosphospecific or total SgK269 antibody. Cell lysates were blotted as indicated. Grb2 served as a loading control.

Figure 2: SgK269 protein expression is elevated in basal breast cancer cell lines and a subset of primary breast cancers. (A) Western blot analysis of SgK269 and Lyn expression across a panel of breast cancer cell lines. (B) SgK269 mRNA expression across breast cancer cell lines. Data are expressed relative to the expression level of MCF-7 cells (Mean ± SEM, n=3). (C) Western blot analysis of SgK269 expression in different subtypes of primary breast cancer.

Figure 3: SgK269 promotes epithelial to mesenchymal transition in MCF-10A cells. (A) SgK269 was stably expressed in MCF-10A cells and cell lysates blotted for the indicated proteins. In the left panel, lysate from MDA-MB-231 basal breast cancer cells was included for comparison. (B) Photomicrographs of MCF-10A cells expressing SgK269 and vector control cells (Scale bar = 50 μm). The histogram on the right indicates mean cell length from the two cell populations (Mean ± SEM, n=100, * = $p < 0.05$). (C) Changes in expression of specific EMT markers induced by SgK269.

Expression of 84 EMT-related genes was quantified by qRT-PCR, and genes exhibiting significant ($p<0.05$) changes in replicate experiments selected. The graphs indicate fold expression changes in genes normally upregulated (top panel) or downregulated (bottom panel) during EMT. (D) Random cell motility of MCF-10A cells expressing SgK269, as determined by live cell tracking (Mean ± SEM, n=50, * = $p < 0.05$). (E) Fluorescence microscopy of MCF-10A cells expressing SgK269, stained with an anti-HA antibody and phalloidin. Scale bar = 10 μm.

Figure 4: SgK269 promotes growth and abnormal morphology of MCF-10A acini. (A) Proliferation of vector control and SgK269 expressing MCF-10A cells determined by MTS assay. Data presented are representative of at least three independent experiments (Mean ± SEM, n=6). (B) Growth of control and SgK269 expressing MCF-10A acini in matrigel. Data shown are representative of at least three independent experiments (Mean ± SEM, n=100, * = $p < 0.05$). (C) Photomicrographs of MCF-10A acini grown in matrigel for 12 d. Scale bar = 100 μm. (D) Fluorescence microscopy of MCF-10A acini grown in matrigel for 12 d and stained with antibodies against E-cadherin and Ki67. Scale bar = 100 μm.

Figure 5: Functional characterization of Lyn phosphosites within SgK269. (A) Expression and tyrosine phosphorylation of Y616F and Y635F mutants in MCF-10A cells. (B) Photomicrographs of cells expressing WT and mutant versions of SgK269. Scale bar = 50 μm. (C) Photomicrographs of acini expressing WT and mutant versions of SgK269. Cells were grown in Matrigel for 12 d. Scale bar = 100 μm. (D) Left histogram:

Quantification of acinar diameter following growth in matrigel for 12 d. Data represent Mean ± SEM, n=100, * = $p < 0.01$ relative to vector control acini. Right histogram: Quantification of MCF-10A acini presenting abnormal, multi-lobular morphology, * = $p < 0.01$ relative to vector control acini. (E) SgK269 enhances cell invasion in a Y635-dependent manner. Data shown are the mean ± SEM of three independent transwell experiments, * = $p < 0.05$ relative to vector control.

Figure 6: Determination of protein-protein interactions and signaling pathways regulated by Y635 phosphorylation. (A) Co-immunoprecipitation studies with WT SgK269. (B) Co-immunoprecipitation of Grb2 and Shc with WT and Y635F SgK269. The histogram provides quantification of the Grb2 interaction with Y635F SgK269 normalised to the respective interaction with WT SgK269. Data represent Mean ± SEM, n=5, * = $p < 0.05$. (C) Effect of the SFK inhibitor PP2 on SgK269/Grb2 interaction. SgK269 immunoprecipitates were Western blotted as indicated. For the experiment from MDA-MB-231 cells, separate immunoprecipitates were Western blotted for pY635 and Grb2, and the loading controls are provided below and above the pY635 and Grb2 blots, respectively. (D) Effect of Lyn knockdown on SgK269/Grb2 interaction. SgK269 immunoprecipitates and corresponding cell lysates were Western blotted as indicated. (E) Phosphorylated Y635 represents a binding site for the Grb2 SH2 domain. In the left hand panel, GST or GST-Grb2 SH2 immobilized on beads was used in pulldown assays from the indicated cell lysates. Bound SgK269 was detected by Western blotting and equal loading confirmed by gel staining with Coomassie Blue. In the right hand panel,

pulldown assays were undertaken in the presence or absence of phosphorylated or non-phosphorylated Y635 peptides.

Figure 7: Functional analysis of SgK269 in MCF-10A and basal breast cancer cells. (A) Signalling pathway activation in MCF-10A cells. Cell lysates from monolayers or 3D cultures grown for 4 d were Western blotted as indicated. Numbers below the panels indicate normalized (relative to total) levels of pStat3, pErk and pAkt, expressed relative to the value for vector controls, which is arbitrarily set at 1.0. (B) MEK inhibition reverses the effect of SgK269 on acinar size. Top left, Western blotting on acinar lysates grown for 4 d in the presence of PD184352 at the indicated concentrations. Right, photomicrographs and bottom left, acinar size quantification, of the corresponding acini grown in Matrigel for 12 d. Data represent Mean ± SEM, n=100, * = $p < 0.05$ relative to vector control acini. Scale bar = 100 μm. (C) Stable SgK269 knockdown in MDA-MB-231 cells induces mesenchymal to epithelial transition. Left hand panel, lysates from control and SgK269 knockdown cells were Western blotted as indicated. Right hand panel, morphology of the corresponding cell pools, as indicated by light microscopy. Scale bar = 50 μm (D) Effect of stable SgK269 knockdown in BT-549 and MDA-MB-468 basal breast cancer cells. Cell lysates were Western blotted with the indicated antibodies. The histogram provides the results for anchorage-independent growth assays where control or SgK269 knockdown BT549 cells were grown in soft agar for 14 d. Data represent Mean ± SEM, n=3, * = $p < 0.05$.

Figure 1

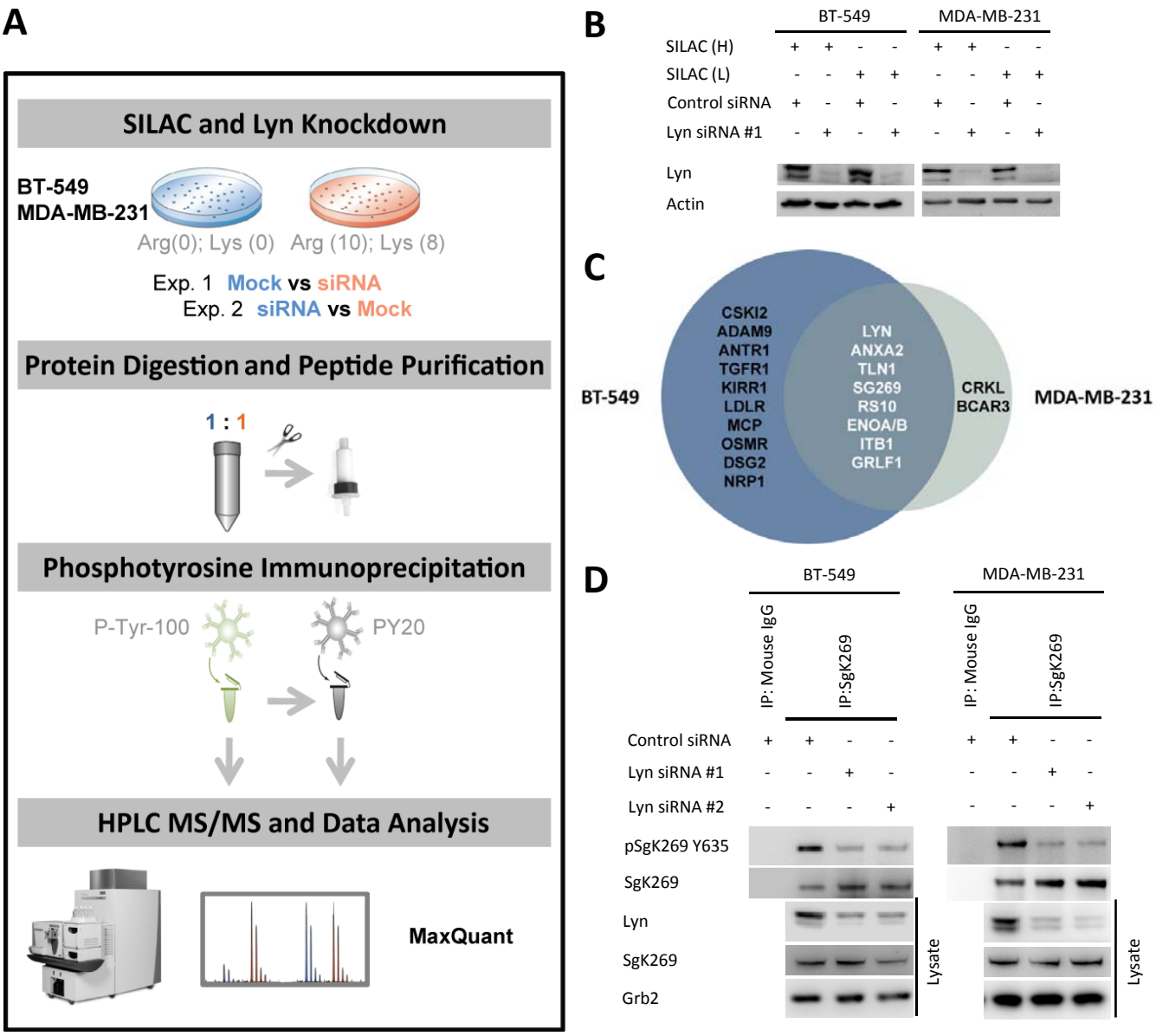
A
SILAC and Lyn Knockdown
BT-549
MDA-MB-231
Arg(0); Lys (0)
Arg (10); Lys (8)
Exp. 1 Mock vs siRNA
Exp. 2 siRNA vs Mock
Protein Digestion and Peptide Purification
1 : 1
Phosphotyrosine Immunoprecipitation
P-Tyr-100
PY20
HPLC MS/MS and Data Analysis
MaxQuant
B
BT-549
MDA-MB-231
SILAC (H)
SILAC (L)
Control siRNA
Lyn siRNA #1
Lyn
Actin
C
BT-549
MDA-MB-231
CSKI2
ADAM9
ANTR1
TGFR1
KIRR1
LDLR
MCP
OSMR
DSG2
NRP1
LYN
ANXA2
TLN1
SG269
RS10
ENOA/B
ITB1
GRLF1
CRKL
BCAR3
D
BT-549
MDA-MB-231
IP: Mouse IgG
IP:SgK269
Control siRNA
Lyn siRNA #1
Lyn siRNA #2
pSgK269 Y635
SgK269
Lyn
SgK269
Grb2
Lysate
Lysate

Figure 2

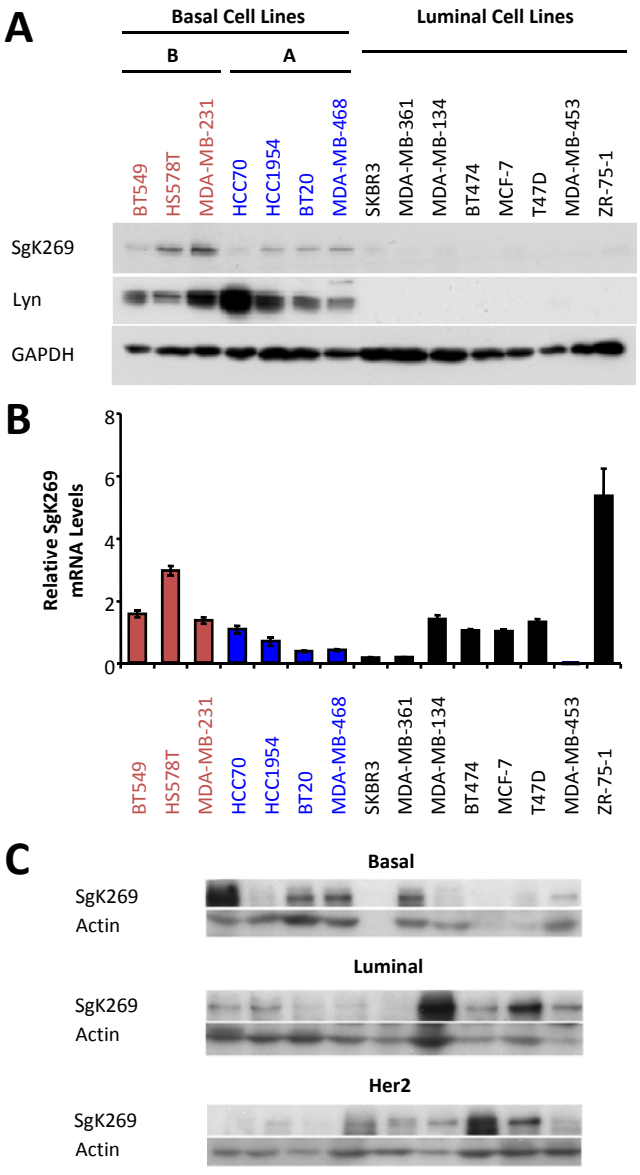
A
Basal Cell Lines
Luminal Cell Lines
B
A
BT549
HS578T
MDA-MB-231
HCC70
HCC1954
BT20
MDA-MB-468
SKBR3
MDA-MB-361
MDA-MB-134
BT474
MCF-7
T47D
MDA-MB-453
ZR-75-1
SgK269
Lyn
GAPDH
B
Relative SgK269 mRNA Levels
0
2
4
6
8
C
Basal
SgK269
Actin
Luminal
SgK269
Actin
Her2
SgK269
Actin

Figure 3

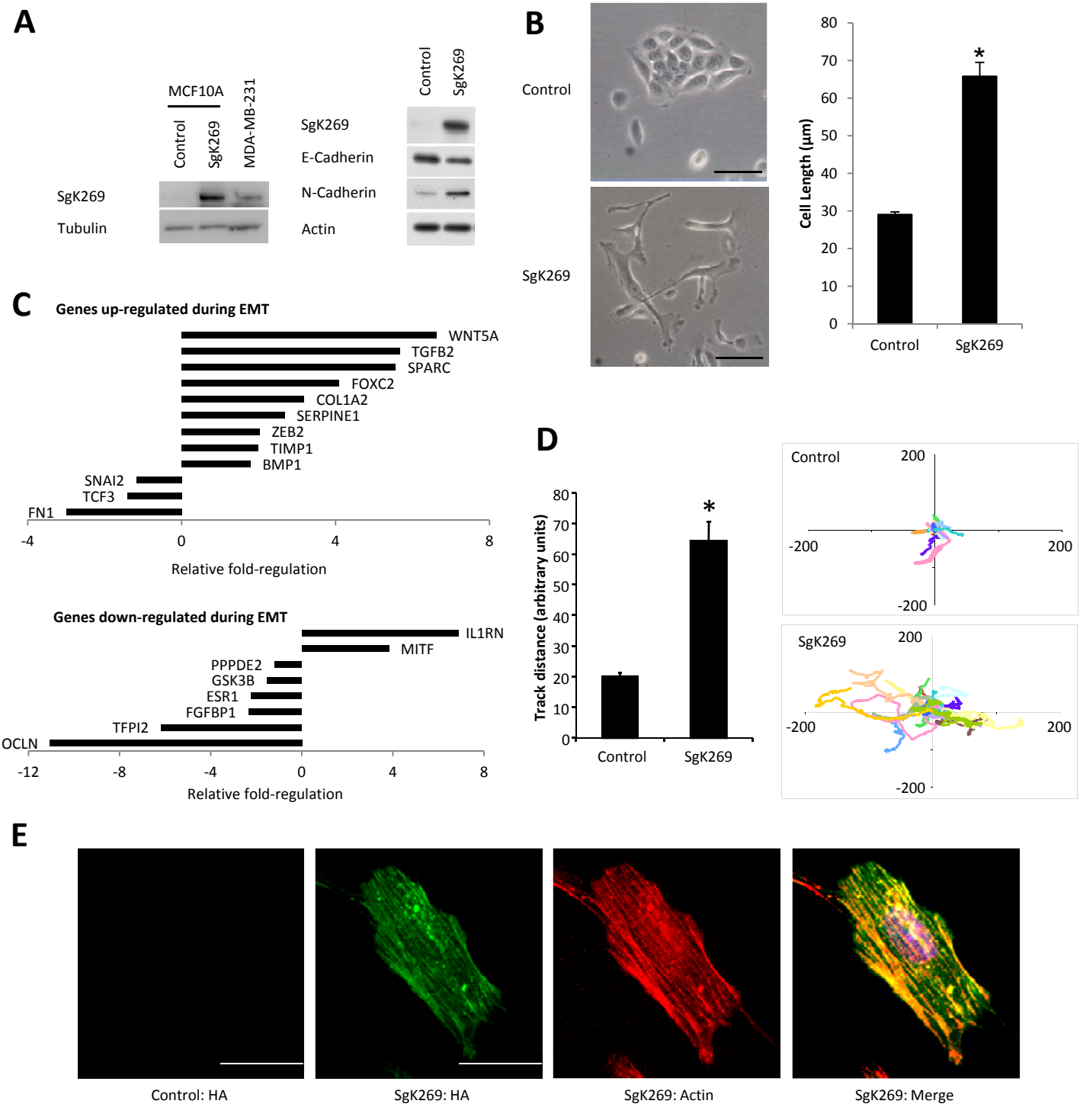
A
MCF10A
Control
SgK269
MDA-MB-231
SgK269
Tubulin
Control
SgK269
SgK269
E-Cadherin
N-Cadherin
Actin
B
Control
SgK269
Cell Length (µm)
80
70
60
50
40
30
20
10
0
*
Control
SgK269
C
Genes up-regulated during EMT
WNT5A
TGFB2
SPARC
FOXC2
COL1A2
SERPINE1
ZEB2
TIMP1
BMP1
SNAI2
TCF3
FN1
-4
0
4
8
Relative fold-regulation
Genes down-regulated during EMT
IL1RN
MITF
PPPDE2
GSK3B
ESR1
FGFBP1
TFPI2
OCLN
-12
-8
-4
0
4
8
Relative fold-regulation
D
Track distance (arbitrary units)
80
70
60
50
40
30
20
10
0
*
Control
SgK269
Control
200
-200
200
-200
SgK269
200
-200
200
-200
E
Control: HA
SgK269: HA
SgK269: Actin
SgK269: Merge

Figure 4

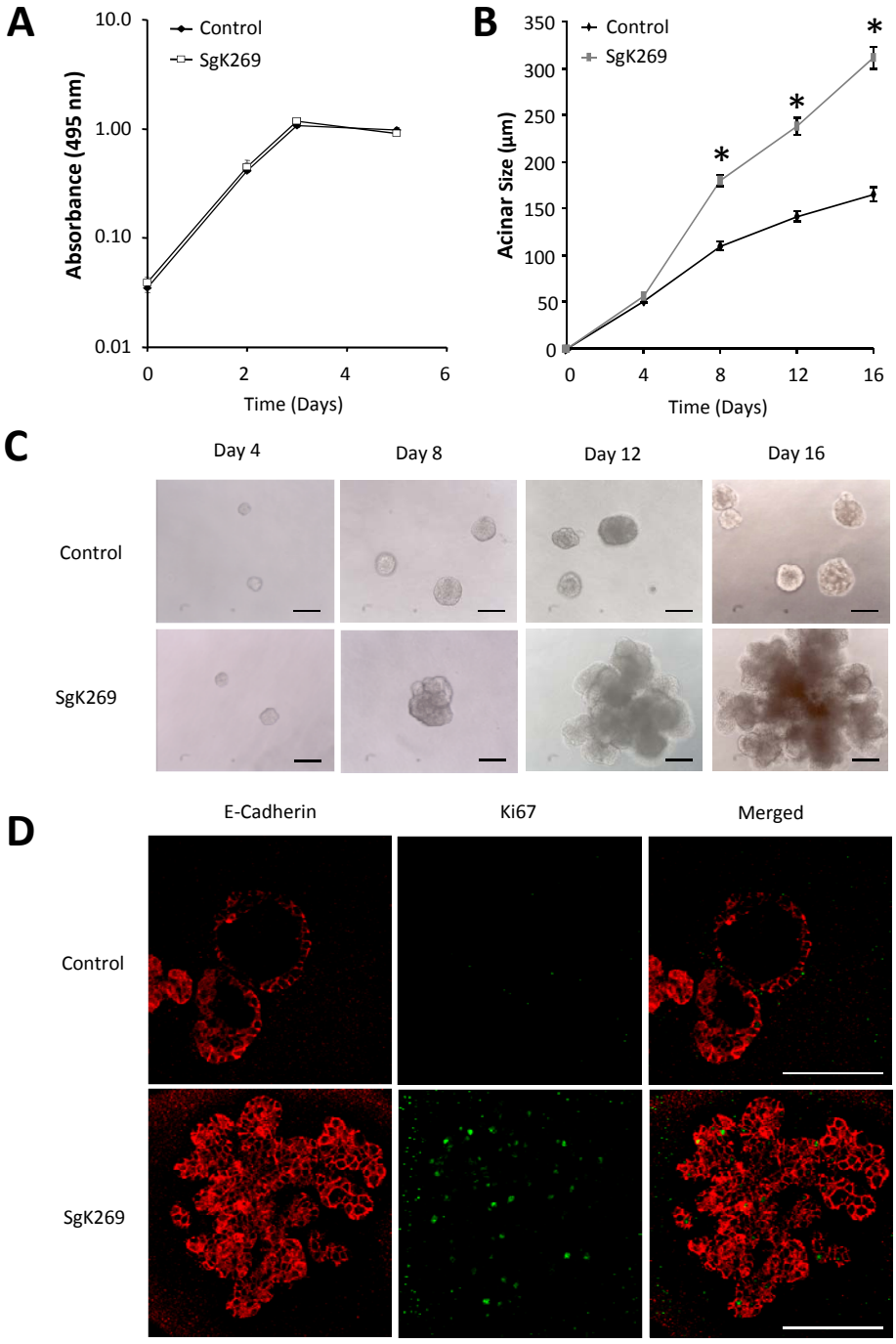
A
Absorbance (495 nm)
10.0
1.00
0.10
0.01
Control
SgK269
0
2
4
6
Time (Days)
B
Acinar Size (µm)
350
300
250
200
150
100
50
0
Control
SgK269
*
*
*
0
4
8
12
16
Time (Days)
C
Day 4
Day 8
Day 12
Day 16
Control
SgK269
D
E-Cadherin
Ki67
Merged
Control
SgK269

Figure 5

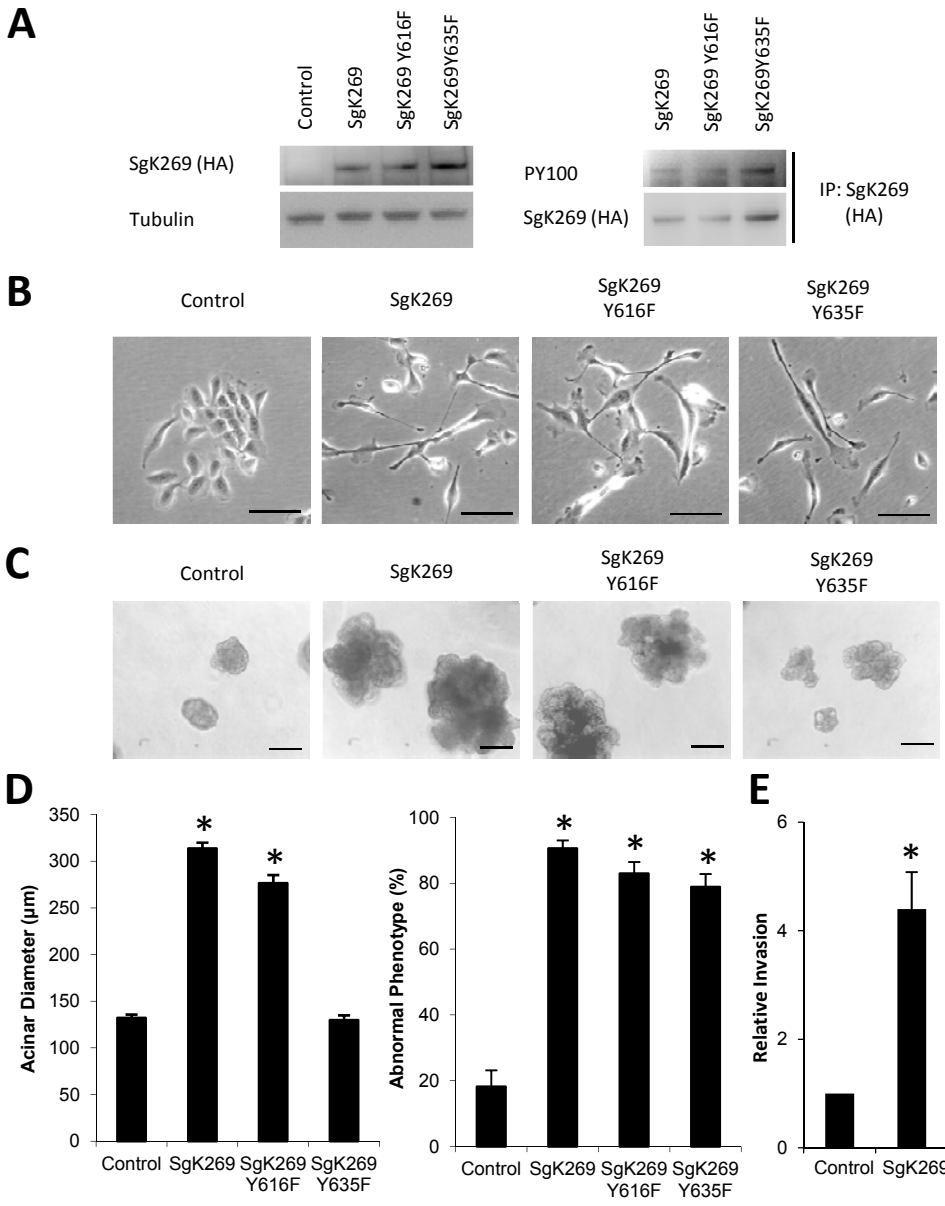
A
Control
SgK269
SgK269 Y616F
SgK269Y635F
SgK269 (HA)
Tubulin
SgK269
SgK269 Y616F
SgK269Y635F
PY100
SgK269 (HA)
IP: SgK269 (HA)
B
Control
SgK269
SgK269 Y616F
SgK269 Y635F
C
Control
SgK269
SgK269 Y616F
SgK269 Y635F
D
Acinar Diameter (µm)
350
300
250
200
150
100
50
0
Control
SgK269
SgK269 Y616F
SgK269 Y635F
Abnormal Phenotype (%)
100
80
60
40
20
0
Control
SgK269
SgK269 Y616F
SgK269 Y635F
E
Relative Invasion
6
4
2
0
Control
SgK269
SgK269 Y635F

Figure 6

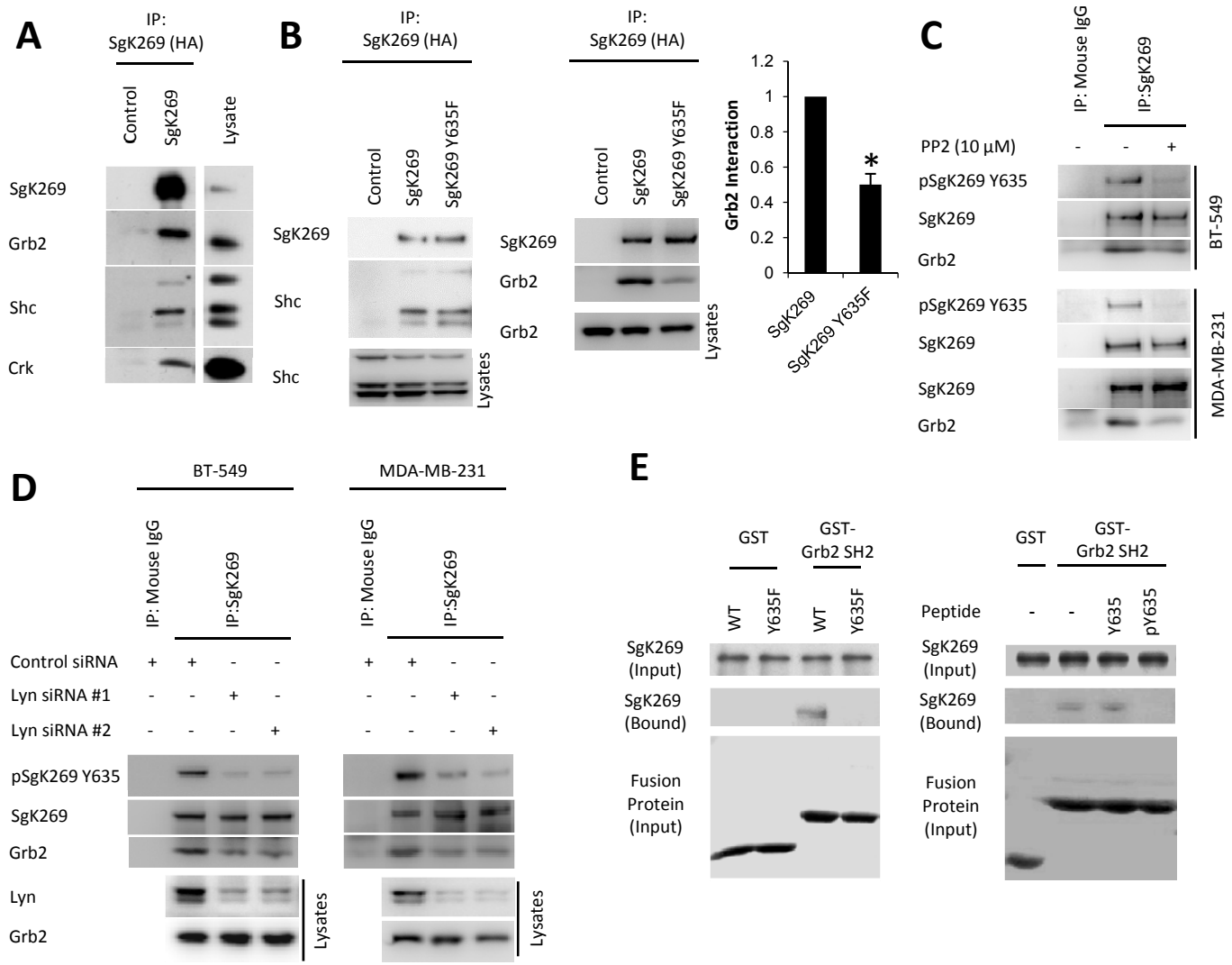
A
IP: SgK269 (HA)
Control
SgK269
Lysate
SgK269
Grb2
Shc
Crk
B
IP: SgK269 (HA)
Control
SgK269
SgK269 Y635F
SgK269
Shc
Shc
Lysates
IP: SgK269 (HA)
Control
SgK269
SgK269 Y635F
SgK269
Grb2
Grb2
Lysates
Grb2 Interaction
1.2
1
0.8
0.6
0.4
0.2
0
*
SgK269
SgK269 Y635F
C
IP: Mouse IgG
IP:SgK269
PP2 (10 μM)
- - +
pSgK269 Y635
SgK269
Grb2
BT-549
pSgK269 Y635
SgK269
SgK269
Grb2
MDA-MB-231
D
BT-549
MDA-MB-231
IP: Mouse IgG
IP:SgK269
IP: Mouse IgG
IP:SgK269
Control siRNA + + - - + + - -
Lyn siRNA #1 - - + - - - + -
Lyn siRNA #2 - - - + - - - +
pSgK269 Y635
SgK269
Grb2
Lyn
Grb2
Lysates
Lysates
E
GST
GST-Grb2 SH2
WT
Y635F
WT
Y635F
SgK269 (Input)
SgK269 (Bound)
Fusion Protein (Input)
GST
GST-Grb2 SH2
Peptide - - Y635 pY635
SgK269 (Input)
SgK269 (Bound)
Fusion Protein (Input)

Figure 7

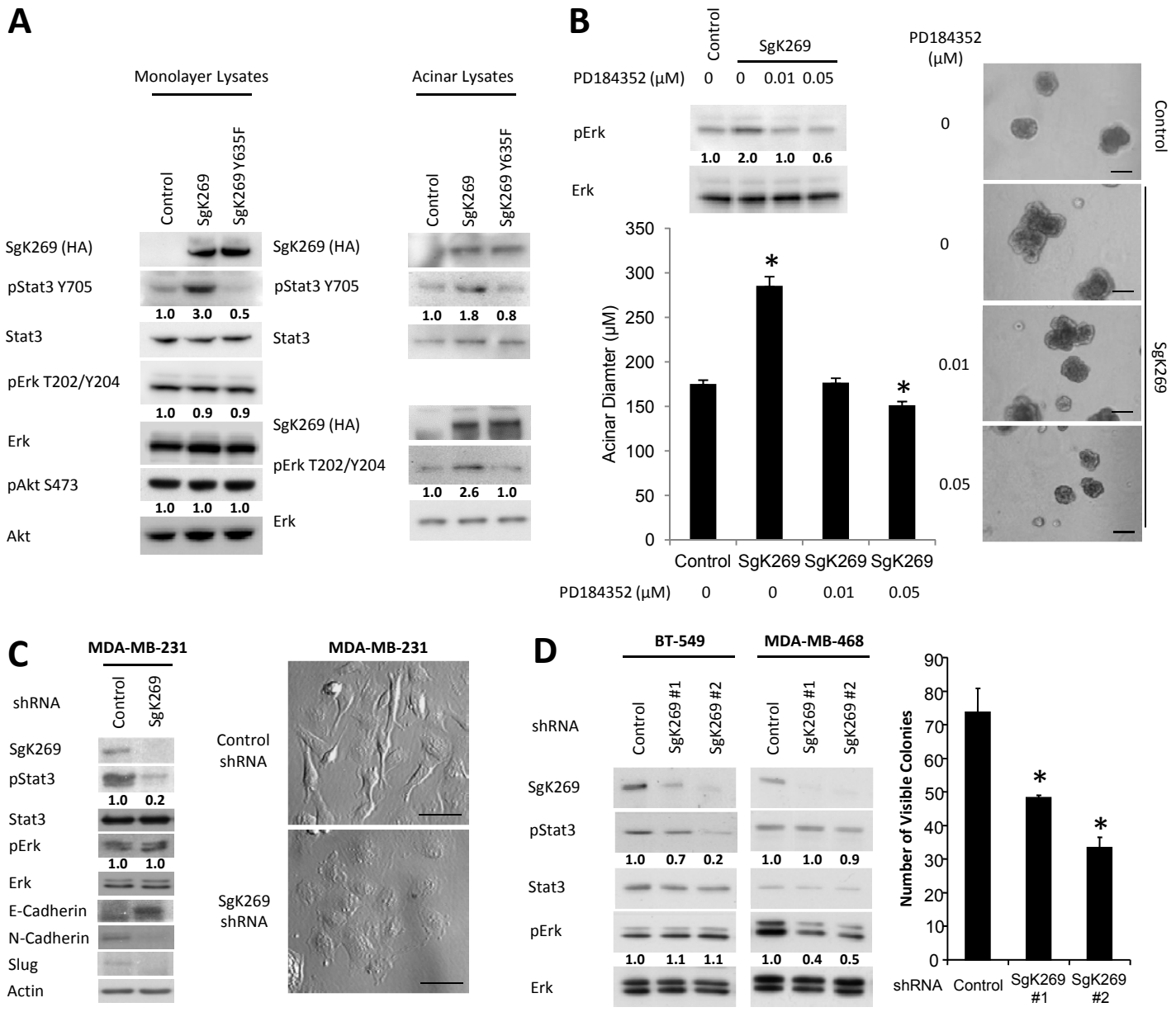
A
Monolayer Lysates
Acinar Lysates
Control
SgK269
SgK269 Y635F
SgK269 (HA)
pStat3 Y705
1.0 3.0 0.5
1.0 1.8 0.8
Stat3
pErk T202/Y204
1.0 0.9 0.9
1.0 2.6 1.0
Erk
pAkt S473
1.0 1.0 1.0
Akt
B
Control
SgK269
PD184352 (μM) 0 0 0.01 0.05
pErk
1.0 2.0 1.0 0.6
Erk
Acinar Diamter (μM)
350
300
250
200
150
100
50
0
Control SgK269 SgK269 SgK269
PD184352 (μM) 0 0 0.01 0.05
PD184352 (μM)
0
0
0.01
0.05
Control
SgK269
C
MDA-MB-231
shRNA
Control
SgK269
SgK269
pStat3
1.0 0.2
Stat3
pErk
1.0 1.0
Erk
E-Cadherin
N-Cadherin
Slug
Actin
MDA-MB-231
Control shRNA
SgK269 shRNA
D
BT-549
MDA-MB-468
shRNA
Control
SgK269 #1
SgK269 #2
SgK269
pStat3
1.0 0.7 0.2
1.0 1.0 0.9
Stat3
pErk
1.0 1.1 1.1
1.0 0.4 0.5
Erk
Number of Visible Colonies
90
80
70
60
50
40
30
20
10
0
shRNA Control SgK269 #1 SgK269 #2